Parallel Imaging with Phase Scrambling

Maxim Zaitsev,[1]* Gerrit Schultz,[1] Juergen Hennig,[1] Rolf Gruetter,[2,3,4] and Daniel Gallichan[2]

Purpose: Most existing methods for accelerated parallel imaging in MRI require additional data, which are used to derive information about the sensitivity profile of each radiofrequency (RF) channel. In this work, a method is presented to avoid the acquisition of separate coil calibration data for accelerated Cartesian trajectories.
Methods: Quadratic phase is imparted to the image to spread the signals in k-space (aka phase scrambling). By rewriting the Fourier transform as a convolution operation, a window can be introduced to the convolved chirp function, allowing a low-resolution image to be reconstructed from phase-scrambled data without prominent aliasing. This image (for each RF channel) can be used to derive coil sensitivities to drive existing parallel imaging techniques. As a proof of concept, the quadratic phase was applied by introducing an offset to the $x^2 - y^2$ shim and the data were reconstructed using adapted versions of the image space–based sensitivity encoding and GeneRalized Autocalibrating Partially Parallel Acquisitions algorithms.
Results: The method is demonstrated in a phantom (1×2, 1×3, and 2×2 acceleration) and in vivo (2×2 acceleration) using a 3D gradient echo acquisition.
Conclusion: Phase scrambling can be used to perform parallel imaging acceleration without acquisition of separate coil calibration data, demonstrated here for a 3D-Cartesian trajectory. Further research is required to prove the applicability to other 2D and 3D sampling schemes. **Magn Reson Med 73:1407–1419, 2015. © 2014 Wiley Periodicals, Inc.**

Key words: parallel imaging; phase scrambling; Fresnel transform; quadratic phase

INTRODUCTION

Since the demonstration of SiMultaneous Acquisition of Spatial Harmonics (SMASH) in 1997 (1), the use of parallel imaging has become ubiquitous through a range of MR applications. The fundamental principle of parallel imaging is to accelerate the encoding process by undersampling k-space while making use of the multiple receive channels of an radiofrequency (RF) array to mitigate the effects of aliasing. Various approaches exist to perform such reconstructions, the best known being the image space–based sensitivity encoding (SENSE) (2) and the k-space based GeneRalized Autocalibrating Partially Parallel Acquisitions (GRAPPA) (3). A property that nearly all parallel imaging techniques share is the requirement to separately acquire additional data containing information about the sensitivity profiles of the RF coils. If it can be assumed that these sensitivity profiles do not change with time then, in principle, a single calibration scan could be performed and used for the reconstruction of a number of subsequent accelerated acquisitions. However, motion of the subject (bulk motion or physiological motion) or scanner instabilities can, especially at higher B_0 fields, compromise the validity of such an assumption. Additionally, the coil sensitivity information must be matched to the field of view (FOV) of the particular acquisition—meaning that practically it has become standard in most cases to incorporate the calibration data into each separate scan. An "autocalibrating" approach is often used, where it is ensured that the central portion of k-space is sampled densely enough to satisfy the Nyquist conditions for the given FOV. These additional k-space samples are often referred to as autocalibration signals (ACS) (4) and can be directly used to derive the kernel for k-space-based methods such as GRAPPA or can be used to generate unaliased low-resolution images from which relative coil sensitivity maps for image-based methods such as SENSE (5) can be derived.

Several recent publications have presented methods that seek to reconstruct both coil calibration data and the final images from the undersampled data themselves (6–9). The price to pay is the increased reconstruction time due to nonlinear iterative methods, typically required for these reconstruction problems. Additionally, all these methods use k-space trajectories with the sampling density increased toward the center of k-space, which essentially contains the required coil calibration information. A method has also been presented (in abstract form), which is capable of resolving Cartesian data undersampled by a factor of 2 without any calibration data at all (10). This was achieved by recognizing that a so-called GRAPPA operator for estimating a missing line of data ($k + 1$) from a neighboring acquired line can also be derived from the square root of the operator, which estimates data across two lines (i.e., estimating line $k + 2$ from line k). The ambiguity of the multiple solutions to the square root, however, requires exhaustive search among all possible solutions for the "correct" one.

It has long been established that imposing a quadratic phase profile across the object leads to the spread of

signals in k-space (phase scrambling), as was originally demonstrated for the purpose of reducing the dynamic range of the acquired signal intensities (11,12). It has also been shown that 1D quadratic phase profiles can be used to suppress signal aliasing (13), leading to more recent work, which demonstrated that 2D phase-scrambled Cartesian undersampled data can be reconstructed using the Fresnel transform without aliasing, but at the expense of image resolution (14). In this article, we demonstrate that an adapted version of this technique can be used as the first stage of a reconstruction of data acquired using an RF array, allowing the synthesis of coil calibration information solely from the undersampled data. Conventional parallel imaging methods can then be applied to complete the image reconstruction pipeline, resulting in an alias-free image with no loss of image resolution—and avoiding the necessity for acquisition of additional RF calibration data. In this proof-of-concept work, quadratic phase within the image is achieved by offsetting the second-order shims. For practical implementations, it would be recommended to use specialized hardware capable of fast switching the non-linear fields (15,16). The main motivation of this work is to demonstrate the technical feasibility of achieving more efficient spatial encoding by combining parallel imaging with nonlinear phase modulation. Parts of this work have previously been published in abstract form (17,18).

THEORY

Rewriting the Fourier Transform as a Convolution

The following section considers 1D spatial encoding of a sample within a homogeneous RF coil, but multidimensional encoding with coil arrays follows as a trivial extension of the described approach.

The k-space signals of a sample with magnetization density $\rho(x)$ ignoring relaxation, B_0 and B_1 inhomogeneities can be expressed as follows:

$$s(k) = \int \rho(x)\exp(-i2\pi kx)\mathrm{d}x$$
$$= \int \rho(x)\exp\left(-i2\pi\frac{k}{k_{\max}}\frac{x}{\Delta x}\right)\mathrm{d}x, \qquad [1]$$

where integration is performed over the sensitive volume of the receiver coil; $k_{\max}$ and Δx are the k-space sampling extent and resolution in image space. Nyquist k-space sampling requires $k_{\max}\Delta x = 1$. On introduction of dimensionless variables

$$\eta = \frac{k}{k_{\max}},\ \xi = \frac{x}{\Delta x}, \qquad [2]$$

and using the trivial substitution

$$2\eta\xi = \eta^2 + \xi^2 - (\eta - \xi)^2, \qquad [3]$$

Equation [1] can be rewritten as

$$s(\eta k_{\max}) = \int \rho(\xi\Delta x)\exp(-i\pi\eta^2)\exp(-i\pi\xi^2)$$
$$\times \exp\left(i\pi(\eta - \xi)^2\right)\Delta x\, \mathrm{d}\xi. \qquad [4]$$

By defining a chirp function $g(\vartheta) = \exp(i\pi\vartheta^2)$, modulated spin density and modulated k-space signal variables can be introduced as

$$\rho'(\xi) = \rho(\xi\Delta x)\Delta x g^*(\xi),$$
$$s'(\eta) = s(\eta k_{\max})\, g(\eta), \qquad [5]$$

which enable us to simplify Eq. [4]. Indeed, modulated signal intensity can now be expressed as a convolution of the modulated spin density with the chirp function as

$$s'(\eta) = \int \rho'(\xi)\exp\left(i\pi(\eta - \xi)^2\right)\mathrm{d}\xi, \qquad [6]$$

or in a shorthand notation:

$$s' = \rho' \otimes g, \qquad [7]$$

where the symbol $\otimes$ denotes the convolution operation. The chirp function used as a convolution kernel in Eqs. [6] and [7] is a pure phase term, which upon using the Fourier convolution theorem and the explicit Fourier transform of a Gaussian function permits the formulation of the image reconstruction in terms of a convolution with a conjugated chirp g^*:

$$\rho' = s' \otimes g^*. \qquad [8]$$

The above derivation of the convolution interpretation of MR image reconstruction is entirely equivalent to the traditional Fourier transform. However, the presence of a convolution with an explicit kernel invites the study of the properties of this kernel in more detail and to investigate the possibilities of changing this kernel to alter the properties of the image reconstruction. It is also noteworthy that Eq. [8] describes a transformation from the frequency domain to the spatial domain without an explicit Fourier transform—instead the original data $s(k)$ are modulated by a chirp function to form $s'(\eta)$, which on convolution with the chirp function g^* gives the desired image of the object $\rho'(\xi)$. The superscript prime is added to represent that this version of the image still has a known chirp-modulated phase—which can be unwound if the phase of the image is of interest.

Suppressing Aliasing with the Convolution Reconstruction

To efficiently calculate Eq. [8], the Fourier convolution theorem may be applied making it equivalent to Eq. [9] in Ref. (14). In analogy with this publication, we consider a convolution kernel modified as

$$g_\alpha(\vartheta) = \exp(i\pi\alpha\vartheta^2), \qquad [9]$$

where α is the scaling parameter, defining the resolution and FOV of the reconstructed image. As we showed previously (17,18), sampling properties such as aliasing can directly be observed from a discretization of the modified kernel in Eq. [9] (see also explanations of Fig. 2). To suppress aliasing with scaled kernels, a further modification of the kernel is required:

$$g_{aw}(\vartheta) = w_\alpha(\vartheta)\exp(i\pi\alpha\vartheta^2), \qquad [10]$$

where $w_\alpha(\vartheta)$ is a window function (normalized to preserve the resulting image intensity). A variety of window
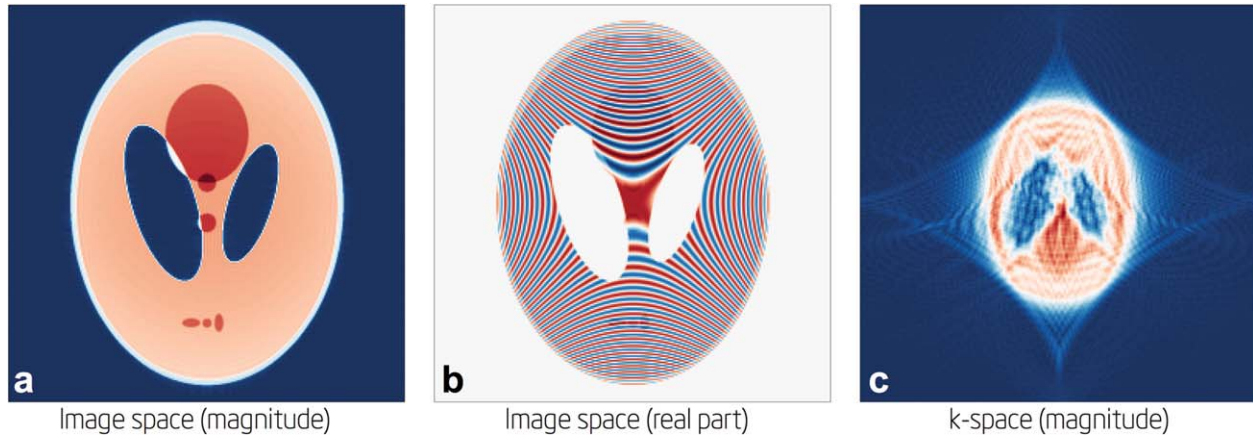
FIG. 1. The simulated object magnitude (**a**) and its real component (**b**), demonstrating the strong quadratic phase variation. **c**: The corresponding magnitude of the k-space.

functions may be used—in this work, we chose a Fermi band-pass filter.

Until the addition of the scaling parameter (α in Eq. [9]), the reconstruction is entirely equivalent to the Fourier transform, but it is the combination of the scaling and windowing that leads to the aliasing-suppression properties of the described reconstruction. A nonwindowed kernel exhibits multiple "centers" due to the undersampling of the discrete quadratic function, which leads to the convolution reconstruction exhibiting the aliasing familiar from the Fourier transform of undersampled data. The alias-free images presented in Ref. (14) appear at first glance to be produced without the need for a windowing function—but by choosing also to replace the convolution in Eq. [9] by a fast Fourier transform (FFT) operation, the method implicitly applies a top-hat filter at the same resolution as the FFT. In this work, we chose to keep the (slower) pure convolution to retain explicit control over the windowing as the spatial extent of the filter proves to be critical in assuring an alias-free reconstruction.

For the convolution reconstruction to achieve suppression of aliasing, it is necessary that the signals originating from different locations in the object are separated in the acquired k-space—which can be achieved by inducing a phase distribution to the object in addition to the primary gradient encoding. This allows the convolution kernel to assimilate signals from the multiple sources aliasing to a particular location with a different weighting—where the amplitude of this weighting depends on the chosen windowing function. The distribution of the shifted signals is also important, as to reconstruct a useful image the bulk intensity component of each spatial location (i.e., the center of the local k-space—which we refer to here as the *principal echo*) must fall within the locus of the windowed kernel from the actual image-space location (see also explanations of Fig. 2). In other words, convolution with the windowed kernel cannot shift signals farther than the locus of that kernel, so each DC component in k-space must already lie within a certain "range" of its final destination in the image—as the convolution with the kernel is the only operation which redistributes signal in this method of moving from

k-space to image space (Eq. [7]). This condition can be expressed mathematically as

$$-W < \left(x \mp \Delta k(x) \right) < W, \qquad [11]$$

where $\Delta k(x)$ is a k-space echo shift for the location given by x, and W is the distance from the window function center to its cut-off edge. Note that all variables in this equation are given in pixels in image space or k-space. This condition must hold across the entire object, and the $\mp$ sign indicates that either the $-$ sign or the $+$ sign must hold everywhere. The $+$ sign is equally valid as it corresponds to the case where the conjugate reconstruction (or flipped image) falls within the locus of the windowed kernel.

The convolution method is only able to resolve aliasing for low spatial-resolution features of the image, as only these signals are contained within a small radius of the principal echo in k-space. Shifting of the echoes in k-space allows the windowed convolution kernel to select only the principal echoes from a certain region in the original object to be able to contribute to the image in a particular location. The higher spatial frequencies, however, are distributed throughout the outer regions of a conventional k-space—and are, therefore, distributed across the entire k-space when phase scrambling has shifted the echoes. The windowed convolution kernel is not able to "reach out" to the "correct" signals for the higher spatial frequencies. This corresponds to the observation in Ref. (14) that aliasing could only be resolved for "zoomed-out" lower-resolution images (when $\alpha > 1$)—as this excludes the higher spatial frequencies.

Choosing the Phase Modulation

For the method to function correctly, it is required to impose a phase modulation in image space which disperses sufficiently the signals in k-space, but that also satisfies Eq. [11]. From the Fourier shift theorem, it is known that the k-space echo shift $\Delta k(x)$ is proportional to the local spatial gradient of the signal phase at position x. Therefore, the simplest phase distribution satisfying our requirements is one where the spatial derivative
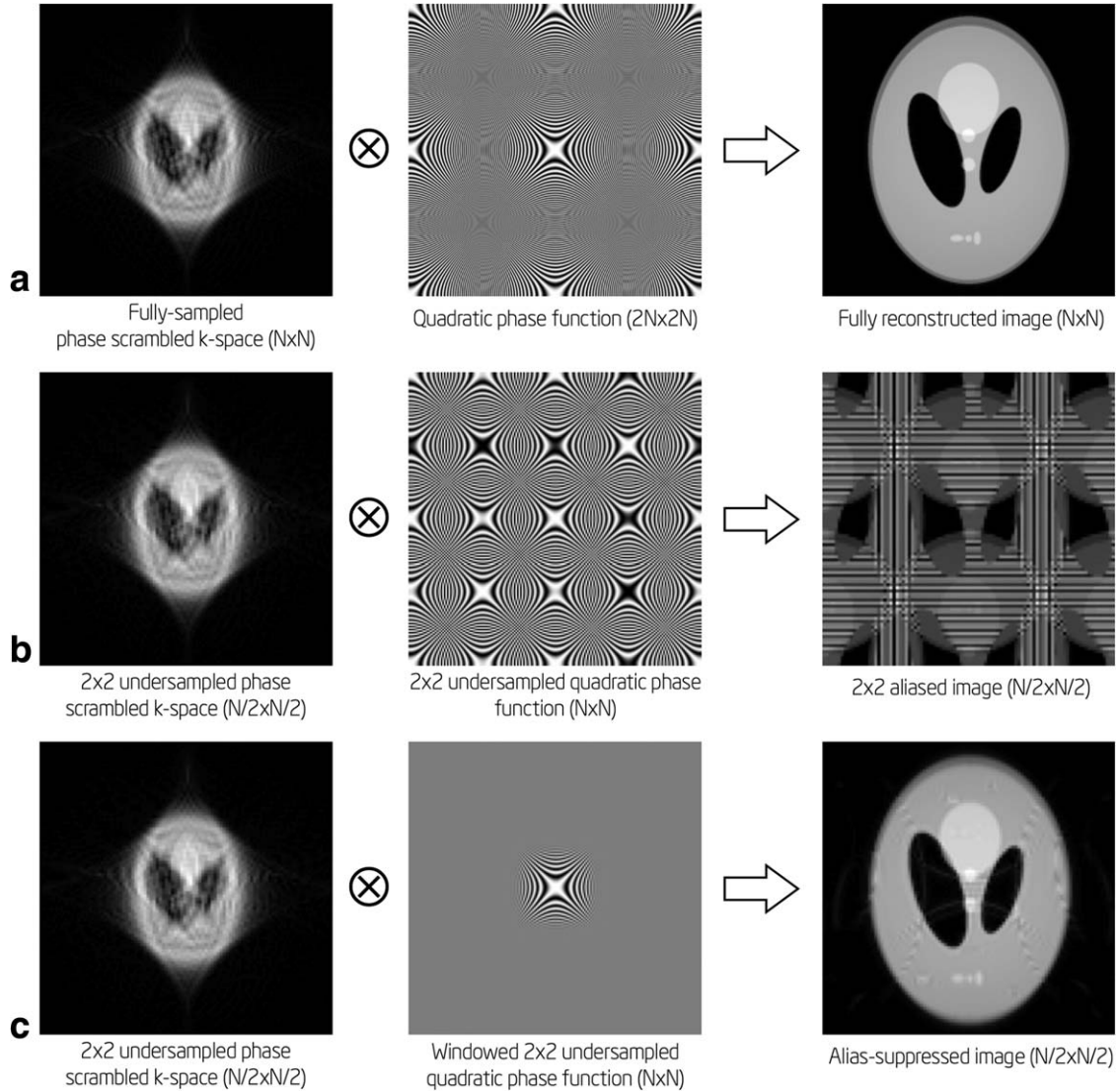
FIG. 2. As described in the text, (**a**) the Fourier transform can be rewritten as a convolution with a quadratic phase function. **b**: When 2 × 2 undersampled phase-scrambled data are reconstructed with this method, the familiar aliasing pattern arises, as expected from the Fourier transform. **c**: If the quadratic phase function is appropriately windowed, however, an alias-suppressed image can be reconstructed. Note that k-space "images" in (b) and (c) are of lower resolution, which corresponds to undersampling without zero-filling the missing lines. Also note that the convolution kernels are of double matrix sizes compared to both k-space and object-space images and have been rescaled in the figure for presentation purposes, whereas actual convolution occurs in the pixel domain.

is proportional to the coordinate itself, such as the quadratic phase function:

$$\psi = \beta x^2, \qquad [12]$$

where β describes the strength of the quadratic modulation. This strength is clearly important as it directly controls the extent of the signal spread in k-space. If the modulation is too weak, aliasing cannot be adequately suppressed. If the modulation is too strong, the edges of the object will not be refocused inside the acquired k-space range and signal dropout will occur [as has been demonstrated for reduced FOV imaging (19)].

A quadratic phase can be introduced to an MR image in a number of ways, such as using tailored RF excitation, e.g., Refs. 12 and 13, or the presence of an additional quadratic B_0 field between excitation and readout

(12). For the current work, we chose to offset one of the second-order shim coils ($x^2 - y^2$) as this was the simplest approach to implement and adequately demonstrate the method. Figure 1 shows a simulated object with phase added in image space following the $x^2 - y^2$ form and the corresponding k-space, where the signals are shifted such that it resembles the object itself. Note that the signal shift in k-space is proportional to the derivative of the phase—and so the negative sign for y in ($x^2 - y^2$) leads to the inversion of the object along the y-axis.

Figures 2 and 3 demonstrate the principle behind the alias-suppression, which results from the convolution reconstruction when applied to phase-scrambled data. Equations [7]–[9] express the Fourier transform as a convolution operation (along with multiplications with chirp functions, which for brevity are not shown in the
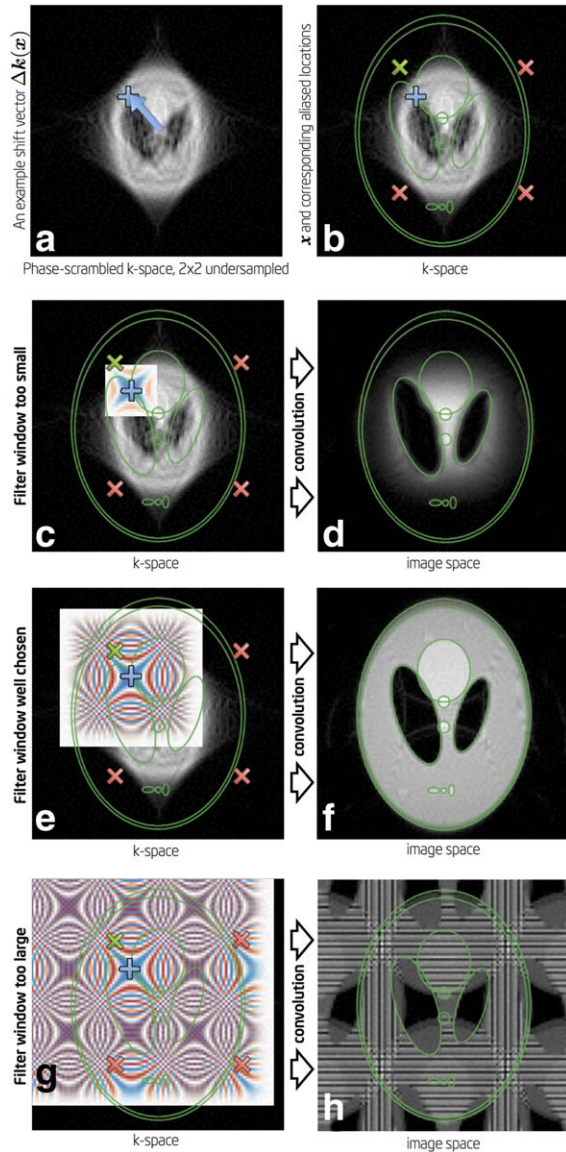
FIG. 3. Diagram demonstrating the importance of the filter window in the convolution reconstruction. **a**: A 2×2 undersampled k-space with quadratic phase scrambling. A vector $\Delta k(x)$ has also been marked, showing the shift of the principal echo for a point in the image located just above the larger of the two "lobes" in the digital phantom. **b**: The same k-space overlaid with the outline of the object in image space. The vector x is indicated with a green cross, and the three locations where it will alias to with 2×2 undersampling are indicated with red crosses. **c**: When the filter window is too small, the green cross falls outside the locus of the convolution kernel when centered on $\Delta k(x)$ leading to an incomplete reconstruction (**d**). **e**: When the filter window is well chosen, the green cross falls within the convolution kernel but the red crosses fall outside of it, leading to the alias-suppressed image (**f**). **g**: If the filter window is too large all four crosses fall within the convolution kernel and the resulting image is aliased as would occur when using an FFT (**h**).

figures). When the k-space data are convolved with a quadratic phase function without windowing (Fig. 2b), the resulting image exhibits the same aliasing as from the Fourier transform, as expected (the quadratic phase function needs to be defined on a $2N \times 2N$ grid to fully define the convolution over the $N \times N$ k-space). With an appropriately sized window on the quadratic phase function, however, the signals corresponding to low spatial frequencies are assigned to their actual location in the final image but are prevented from appearing at their three aliased locations as these fall outside the locus of the windowing function from the phase-scrambled k-space (Fig. 2c). To demonstrate this effect in more detail, Figure 3a shows the 2×2 undersampled phase-scrambled k-space with an example shift-vector $\Delta k(x)$ where the location has been selected to be easily identifiable by eye slightly above the larger of the two "lobes" of the digital phantom. Figure 3b shows the same undersampled k-space with an overlay of the outline of the digital phantom in image space. The green cross indicates the location x in image space for which the principal echo will have been shifted by $\Delta k(x)$. The red crosses indicate the image-space locations where aliasing of the location x will occur for 2×2 undersampling. Figure 3c and d shows that if the filter window of the convolution kernel is too small there is no way for the principal echo to be correctly located onto the desired location x. When the window size is well chosen, the kernel reaches the desired location x but does not reach any of the aliased locations (Fig. 3e,f). If the filter window is too large, however, the kernel reaches the desired location and the aliased locations, thereby reproducing the aliasing artifact expected from a Fourier reconstruction.

The convolution reconstruction is, therefore, able to strongly suppress aliasing of low-resolution features of the object, but some artifacts resulting from aliasing of higher spatial frequencies remain (the residual aliasing visible in Figs. 2c and 3f). It should be noted that for clarity the y-direction of the k-space images has been reversed with respect to Figure 1—whereas during the actual reconstruction the flipping of y-direction of the k-space representation of the object (resulting from the $x^2 - y^2$ phase distribution) was handled using a 2D chirp function where the polarities were opposite for the x- and y-dimensions.

An important question is the choice of the optimal parameter β in Eq. [12], which controls the achievable image-space resolution in the low-resolution convolution reconstruction. The induced phase dispersion should, therefore, be large enough for the low-resolution alias-suppressed reconstruction to capture the spatial distributions of the coil sensitivities, but not so high as to avoid signal suppression mentioned above.

Creating the Final Reconstructed Image

The convolution reconstruction described so far is only capable of resolving the aliasing for the low spatial-resolution features of the image—aliasing of high spatial-resolution features will remain. If desired, this residual aliasing can also be suppressed by spatial smoothing, but this will necessarily reduce the resolution of the final image. Therefore, we propose to take advantage of the property that the RF coil sensitivity profiles are smoothly varying functions in space—and therefore, should be well described by the low-resolution alias-free

reconstruction offered by the convolution reconstruction. Once low-resolution alias-free images can be reconstructed for each RF coil then sufficient information is available to perform conventional parallel imaging reconstruction methods such as SENSE or GRAPPA—the validity of which should not be affected by the phase scrambling in the data. The result will be a full-resolution image without the need for separate acquisition of coil calibration data—a method we refer to as parallel imaging with phase scrambling (PIPS).

METHODS

Simulations

A digital phantom shown in Figure 1 with a strongly varying quadratic phase (of the form $x^2 - y^2$) was simulated on a matrix of size 792×792 for a Cartesian trajectory of dimensions 192×192, with eight RF coil channels derived from application of the Biot–Savart law. Simulations of the convolution reconstruction were performed for a range of quadratic phase modulations and widths of the Fermi filter used as the windowing function of the convolution kernel ($w_\alpha(\vartheta)$ in Eq. [10])

In Vivo Experiment

To demonstrate the feasibility of the method on in vivo data, we acquired a fully sampled 1-mm isotropic 3D gradient-recalled echo (3D-GRE) dataset (TE/TR = 5.0/6.7 ms) on a single healthy subject on a 7T head-only MR system (Siemens Healthcare, Erlangen, Germany) using a 32-channel receive RF coil (Nova Medical Inc., Wilmington, MA) in accordance with guidelines of the local Ethics Committee. The matrix size was $256 \times 256 \times 176$ with the readout direction chosen to be along the z-axis of the scanner so that the quadratic phase induced by the $x^2 - y^2$ shim coil spread the k-space signals in the two phase-encoding directions. After a normal shimming procedure, the values for the $x^2 - y^2$ shim were manually offset by 6.0 mT/m^2 compared to the optimal shim setting. Nonselective excitation was used for the 3D readout to avoid distortion of the excitation slab resulting from the shim offset. The total scan duration was 5 min and 2 s.

It should be noted that due to the absence of rapidly switchable second-order fields on our system, a shim offset was present throughout the entire pulse sequence. For the simulation, however, we assume that the quadratic background phase has been imparted to the object without significantly affecting the readout itself—thereby making the results independent of the particular pulse sequence used.

An FFT was applied along the readout direction so that the rest of the reconstruction could be treated as a set of independent 2D datasets, one for each slice. The convolution reconstruction was performed as for the simulations, but with the width of the filter window fixed—chosen to cover approximately half of the width of the k-space data in both phase-encoding dimensions.

Phantom Signal-to-Noise (SNR) Experiment

We performed experiments in a phantom (17-cm-diameter sphere filled with doped water) where a series

of 20 volumes were acquired—at a reduced resolution to keep a reasonable total scan time and data volume (2-mm isotropic resolution, $128 \times 128 \times 88$ matrix, TE/TR = 1.25/2.30 ms, 26 s per volume). The acquisition was repeated twice: without and with the quadratic phase. The same quadratic shim offset was used as for the in vivo experiment (6.0 mT/m^2) which, after accounting for the change in matrix size and the change in TE, leads to the signals being spread by the same proportion across the acquired k-space. These data were then used to compare the SNR in various reconstructions after retrospective decimation of the data to simulate undersampling, with and without the presence of the quadratic phase scrambling.

PIPS-SENSE and PIPS-GRAPPA

Once low-resolution alias-suppressed images have been generated, a variety of options are available to perform the standard parallel-imaging reconstruction. For PIPS-SENSE, we first estimated coil sensitivities directly from the windowed convolution reconstruction. As expected, this led to unreliable sensitivity maps in the regions where the convolution reconstruction still shows residual aliasing. To reduce this bias, we then masked out regions where the residuals where greater than 10% of the maximum image intensity and performed fitting of a smooth surface only within the mask using a smoothness parameter to penalize variations in the gradient of the fitted surface (http://www.mathworks.com/matlabcentral/fileexchange/8998-surface-fitting-using-gridfit). During preliminary tests, a value for the smoothness parameter was determined by trial and error, then kept constant for all the data shown. For comparison with the best results we could expect to achieve with PIPS-SENSE, we also performed a SENSE reconstruction where the coil sensitivities were determined by the same smooth fitting procedure but based on the images from the fully sampled data.

To perform PIPS-GRAPPA we required a method to generate the kernel weights for the GRAPPA reconstruction. We found that a simple and reliable method was to unwind the phase of the convolution reconstructed images relative to the first coil channel to remove the quadratic phase from all channels while preserving the relative phase differences and take the FFT. This then gives a "pseudo" k-space where the signals are not spread. We used the central portion (40 samples per accelerated dimension) to derive GRAPPA kernel weights in the standard way. The GRAPPA kernel covered 4×4 samples in two phase-encoding directions, thus providing 16 source points and three target points per RF coil in each instance of the kernel (for the 2×2 acceleration). It was found that for the in vivo data a noticeable improvement was observed when an additional Tikhonov regularization parameter was introduced when deriving the kernel weights from the pseudo-k-space of the convolution reconstructed images.

Preliminary results demonstrated that the determination of the GRAPPA weights from the filtered convolution reconstruction (which still has aliasing for high spatial frequency information) can still lead to residual aliasing artifacts in the final reconstruction. These

artifacts were found to be significantly suppressed with the introduction of an iterative approach to determine the GRAPPA weights, inspired by existing iterative approaches for conventional GRAPPA reconstructions (20). After the PIPS-GRAPPA reconstruction described above, the reconstructed images were again phase unwound with respect to the first RF coil and then Fourier transformed to create a new pseudo-k-space from which new GRAPPA weights could be derived and then applied to the original undersampled data to create a new GRAPPA reconstruction. In total, four such iterations were performed, as for all slices it was found that the procedure had converged by the fourth iteration.

For comparison with the best reconstruction we could expect to achieve with GRAPPA, we derived GRAPPA weights from the fully sampled data. It should be noted that when performing conventional GRAPPA on phase-scrambled data, it is necessary to use the whole of k-space for calibration, as using only a fixed number of central ACS lines will bias the weights to certain regions of the object due to the dependence of the position of signals in k-space on their spatial location in object space.

RESULTS

Simulations

Figure 4, while mainly illustrating the steps of the method, also shows real reconstructions using the proposed method (only the images of the undersampled k-space data have been represented at 32×32 resolution instead of 192×192 so that both the image features and undersampling are still recognizable). The final reconstruction is the (root) sum-of-squares from the individual GRAPPA reconstructions. Although the reconstruction algorithm may be run iteratively, the image in Figure 4c was reconstructed without applying any iterations. It can be seen that the final reconstructed image is of high resolution (the small features within the digital phantom can be clearly recognized) and there is little evidence of aliasing.

Figure 5 demonstrates the importance of choosing the appropriate width of the filter for the windowed convolution, as well as the effect of changing the amount of quadratic phase added for phase scrambling. Without quadratic phase no spreading of the signals in k-space occurs, therefore the convolution reconstruction only reduces the effective FOV of the reconstructed image—but there is no improvement in aliasing. At the other extreme, when the quadratic phase is too strong, the signals are spread so far in k-space as to never be refocused towards the edge of the FOV—leading to signal dropout at the periphery. Decreasing the width of the filter is unable to recover these signals. However, if the strength of the quadratic phase is chosen such that the spread signals cover approximately half of the k-space then the value of the filter window can be seen more clearly. Here, when no window is applied, the aliasing remains—but when the window size is reduced the aliasing becomes effectively suppressed for the low spatial frequency components of the object. Further decreasing the window size leads to signal loss toward the edges of
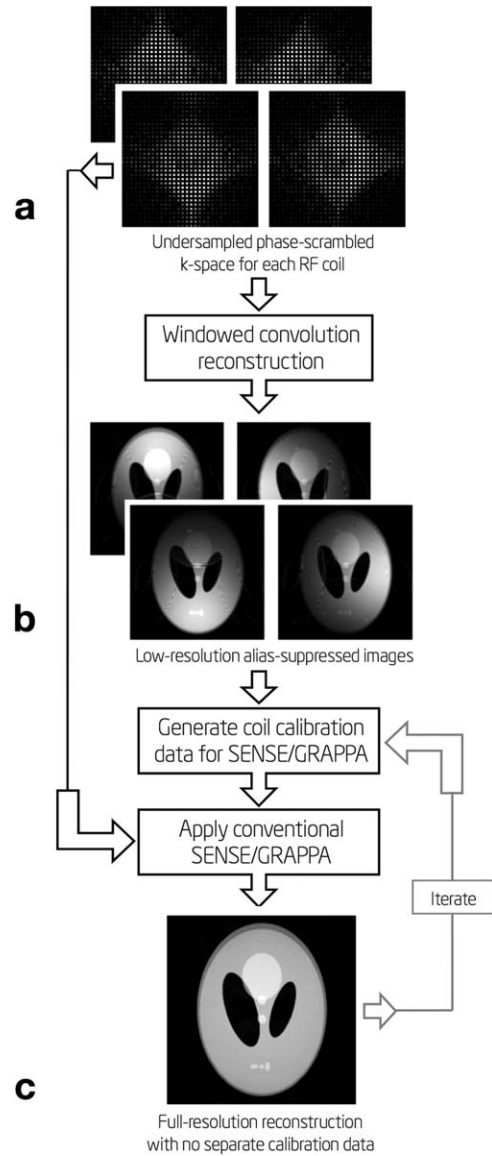

FIG. 4. Flow chart showing the proposed reconstruction method. Undersampled phase-scrambled data **(a)** are reconstructed with the windowed convolution to give low-resolution but alias-suppressed images for each RF coil **(b)**, which can be used to derive the coil sensitivities. The original data can then be reconstructed using conventional parallel imaging methods such as SENSE or GRAPPA to the final image **(c)** without the need for separate acquisition of coil calibration data. If required, the final steps can be iterated by estimating a new set of coil calibration data from the latest reconstructed image.

the object. It should be noted that for all images in this figure, the zoom factor α in Eq. [9] was set equal to 2. Increasing α would also allow alias-suppressed reconstructions for lower values of quadratic phase, but at the expense of the spatial resolution of the convolution reconstruction. The optimal strength of quadratic phase (i.e., the parameter β in Eq. [12]) appears to be when the spread of signals in k-space covers approximately half of k-space—so when designing a protocol it may be necessary to perform preliminary tests to verify that this is being achieved, as changing parameters such as FOV
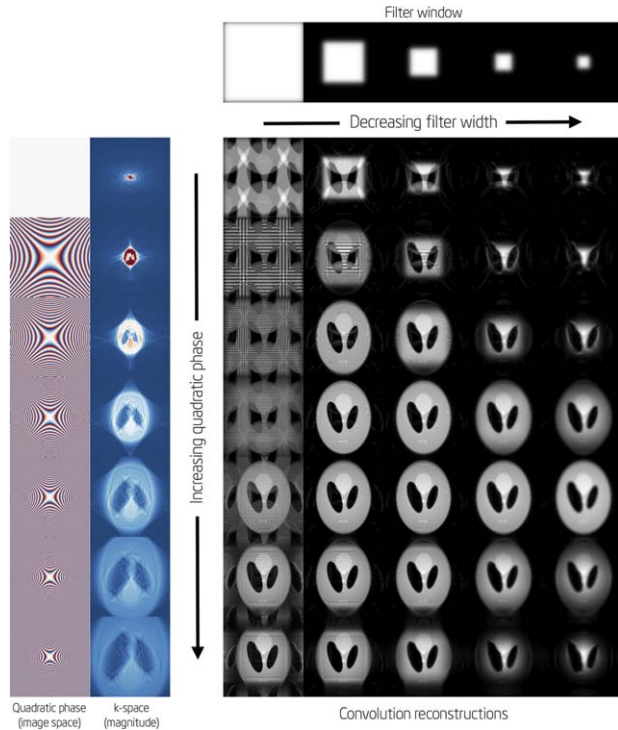
FIG. 5. The effects of increasing the strength of the quadratic phase variation and decreasing the filter window width for the convolution reconstruction of 2 × 2 undersampled data. With no filter window the convolution reconstruction is equivalent to the Fourier transform. With too little quadratic phase the reconstruction is incomplete, and with too much the edges of the object suffer from signal dropout. Note that here the scaling parameter (α in Eq. [9]) was equal to 2. Increasing α would allow alias-suppressed reconstructions for lower values of quadratic phase (at the cost of spatial resolution).

and/or image resolution will also alter the strength of quadratic phase required. As demonstrated in Figure 5, there is a range of values of α and β which lead to a good suppression of aliasing in the convolution reconstruction.

In Vivo Experiment

Figure 6a shows the magnitude of k-space (after an FFT along the readout direction, z) for the 3D-GRE data collected in vivo with the offset $x^2 - y^2$ shim to spread the signals. Although not as obvious as for the simulated phantom, the shape of the brain is clearly discernible. Note that in Figure 6a, the transversal orientation corresponds to 2D k-space, whereas the sagittal and coronal orientations correspond to hybrid spaces with the head–feet direction already Fourier-transformed. For reference, Figure 6b also shows the direct FFT reconstruction of the data from Figure 6a after decimation to 2 × 2 acceleration in the two phase-encoding directions. Figure 6c then shows the same data reconstructed with the windowed convolution method, where it is clear that the aliasing of the low spatial frequencies has been almost completely suppressed. Only minor folding of the high-resolution features (especially the edge of the skull) can

be identified. The expected loss of spatial resolution in the convolution reconstruction is also directly observed.

Figure 7 compares five axial slices out of the 2 × 2 undersampled 3D dataset, which have been reconstructed using SENSE and GRAPPA (both of which require additional data from the fully sampled dataset) and PIPS-SENSE and PIPS-GRAPPA that derive the coil sensitivity information directly from the undersampled data. For all of the reconstructions, the difference from the FFT reconstruction of the fully sampled data is also shown. The residuals from the SENSE and GRAPPA reconstructions are mostly noise-like (although there is a faint low-frequency ringing toward the front of the brain), indicating that the presence of the quadratic phase has not significantly compromised the reconstruction. Over most of the brain, the residuals from the PIPS-SENSE and PIPS-GRAPPA reconstructions are also noise-like—but there are some noticeable localized regions. Especially PIPS-SENSE shows some residual aliasing (Fig. 7c,d), where it mostly follows the regions where the skull is aliased (also the regions of most pronounced aliasing in the windowed convolution reconstruction, Fig. 6c). For PIPS-GRAPPA (Fig. 7g,h), the most noticeable region of significant aliasing is close to one of the eyes—and the aliasing falls outside of the brain. Figure 8 shows orthogonal views of the PIPS-GRAPPA reconstruction of the 2 × 2 undersampled data to demonstrate that the method performs well across the entire brain.

Figure S1 (Supporting Information) shows the improvements to the final reconstruction, which are achieved when including Tikhonov regularization in the derivation of the GRAPPA weights and when using the iterative approach to refining the GRAPPA weights. Four iterations were sufficient for this dataset to suppress the residual aliasing artifacts to the level where they are barely discernible in the final image.

Phantom SNR Experiment

Figure 9 shows reconstructed images of the phantom using conventional GRAPPA and SENSE on data collected with and without phase scrambling. For GRAPPA, no difference between the images is noticeable by eye, but examination of the difference images reveals that the quadratic phase has introduced a small amount of ringing with amplitude approximately 2% of the mean signal. There are small differences in the measured standard deviations—for GRAPPA all values are slightly lower with quadratic phase (by up to ~6%), for SENSE all values are slightly higher (by up to ~4%).

Figure 9 also shows PIPS-GRAPPA and PIPS-SENSE reconstructions for the data acquired with phase scrambling. At 1 × 2 acceleration, they are both indistinguishable by eye from the other reconstructions, although the mean value for PIPS-SENSE is reduced by ~6% (which is also true for the 1 × 3 and 2 × 2 accelerations). At the higher acceleration factors, some horizontal and/or vertical banding artifact is visible within regions where the aliased image overlaps the object itself in both the PIPS-GRAPPA and PIPS-SENSE reconstructions, which have an amplitude approximately 6% of the mean signal.
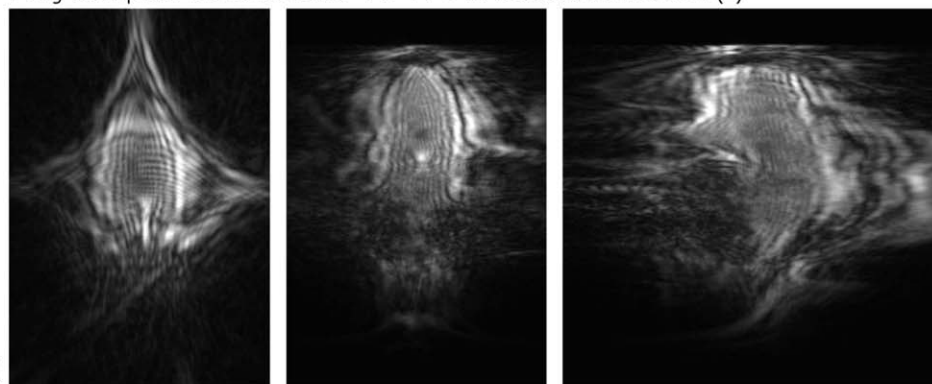
FIG. 6. **a**: Orthographic views of k-space magnitude of in vivo spread-signal 3D-GRE data after FFT along readout direction (*z*). **b**: Sum-of-squares of direct FFT reconstruction of 2×2 undersampled data and **(c)** the same undersampled data following a windowed convolution reconstruction. Note that images in (a) appear flipped along the AP-direction as is to be expected for the $x^2 - y^2$ phase modulation (mostly apparent for the sagittal orientation).
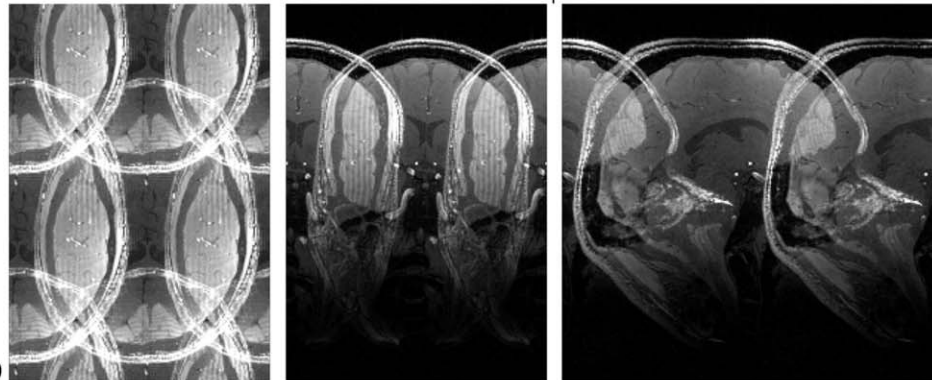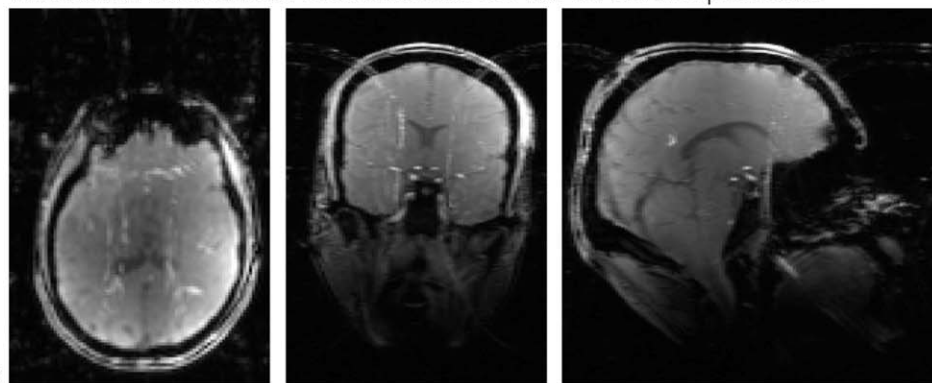
Values of the standard deviations for both PIPS-GRAPPA and PIPS-SENSE are similar to the corresponding GRAPPA and SENSE reconstructions without phase scrambling.

DISCUSSION

We successfully demonstrated that the proposed method is capable of reconstructing accelerated Cartesian data at a variety of 1D and 2D acceleration factors without the need for the separate acquisition of data to calibrate the RF coil sensitivities. The quality of the PIPS-GRAPPA reconstruction within the brain is comparable to that of the reference GRAPPA reconstruction (where the kernel weights were derived from the fully sampled data) but

there are localized regions of aliasing, especially outside of the brain. The PIPS-SENSE results are slightly inferior to the PIPS-GRAPPA, with localized aliasing artifact occurring in some places within the brain as well.

The data from the phantom experiment demonstrate that the introduction of the quadratic phase at this amplitude can cause some minor ringing but has little effect on the SNR. The appearance of the mild banding artifact, especially at higher acceleration factors, is clearly undesirable. However, as this artifact is also apparent in the SENSE reconstructions with quadratic phase—but not in the GRAPPA reconstructions with quadratic phase—it implies that this is the result of small residual deficiencies in the approximation of the coil sensitivities. Therefore, this should not be seen as a
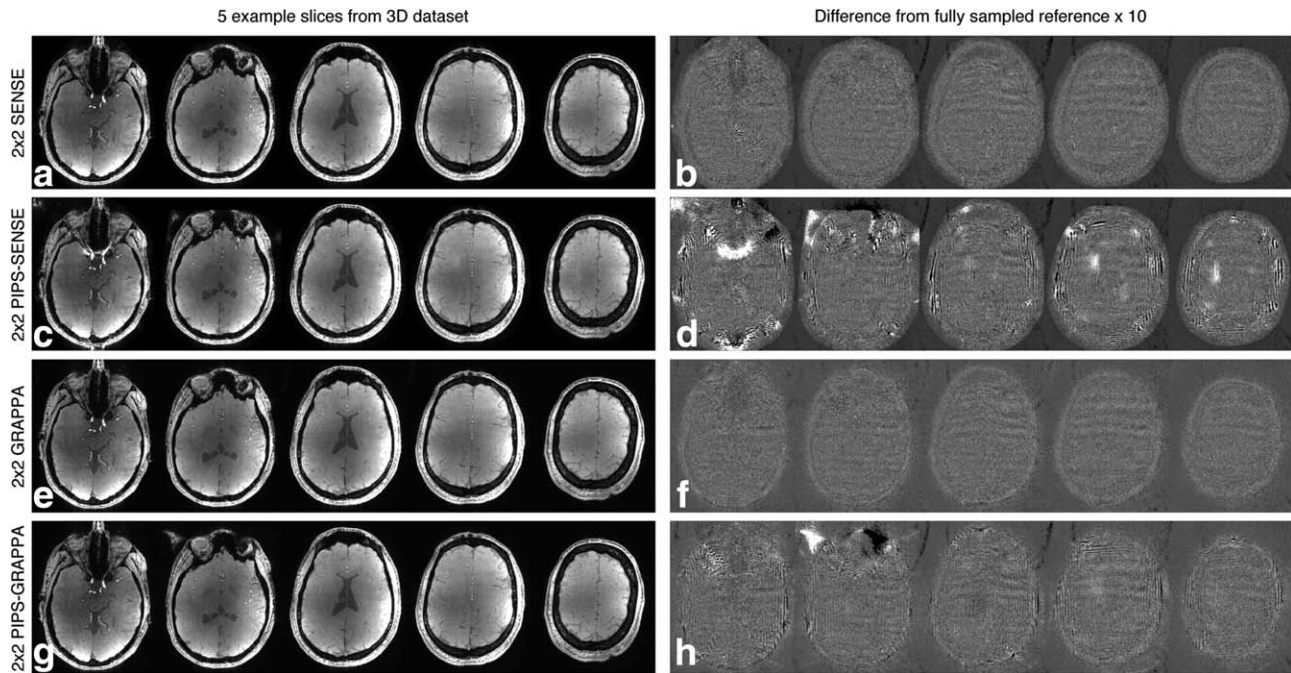
5 example slices from 3D dataset   Difference from fully sampled reference x 10

FIG. 7. (Left column) Reconstruction of the 2 × 2 phase-scrambled undersampled data shown in Figure 6 using SENSE and GRAPPA (which both require coil sensitivity information from the fully sampled data) and PIPS-SENSE and PIPS-GRAPPA (which both derive the coil sensitivity information directly from the undersampled data itself). (Right column) Differences of each of the reconstructions on the left from the FFT reconstruction of the fully sampled data (color scale multiplied by 10 compared to the left column).

limitation of the PIPS methodology per se, as we have demonstrated that a good initial estimate of coil sensitivities can be obtained without ACS lines, but there is still room for future improvement in the refinement process.

For practical imaging situations (such as the matrix size used here of 256 × 256 × 176 and an ACS region of 24 × 24) the PIPS method would allow one to achieve the true net acceleration factor of 4.0 instead of 3.85 (when including the time to acquire the ACS lines). This gain for higher acceleration factors and 2D imaging is even greater because of the increase of the relative contribution of the tightly sampled ACS block to the total scan time. With custom hardware to create the quadratic phase dispersion, PIPS can also be used for 2D imaging. For a 2D image with a matrix size of 128 × 128 and 24 ACS lines, an undersampling factor of 3 results in a net acceleration of 2.2. In this example, PIPS would allow for a choice between achieving the real acceleration factor of 3.0, or gaining some image quality while only slightly increasing the imaging time by lowering the undersampling factor to 2 and thus avoiding some of the g-factor penalty.

We imparted the quadratic phase on the object by offsetting the $x^2 - y^2$ shim as this was the simplest approach to implement and demonstrate the method. This is also readily repeatable on most clinical scanners with no modification necessary—although at lower field strengths it may be necessary to extend the TE further to allow sufficient quadratic phase to accumulate in the object as the available shim strength is often also lower. With standard hardware the method is, therefore, restricted to the use of GRE-based sequences (as the shim offset to impart the quadratic phase is present

throughout the entire pulse sequence) and nonselective RF excitations (as the offset shim will affect the slice-excitation profile). Strongly B_0-sensitive sequences such as EPI or bSSFP would require the quadratic field term to be switched off during the readout module to give usable image quality. Having an offset field applied permanently may also cause some problems with RF excitation profiles—and the quadratic phase will also continue to accrue during the readout itself. Dynamically controllable shim coils (21), or even custom-built inserts (16), would allow the phase to be imparted during the phase encoding or the signal weighting period, but switched off during the RF transmission and readout. This would make the PIPS method applicable to virtually any pulse sequence desired.

Quadratic phase can also be generated using RF pulses (13), but this typically requires longer duration RF pulses than might be convenient. This may, however, be improved using parallel transmission techniques to accelerate the excitation pulse. However, for 2D acceleration during signal reception as demonstrated in this article, a 2D selective RF excitation would be required, and even with parallel transmission acceleration we would still expect the pulse duration to exceed ranges acceptable for the majority of applications.

The PIPS principle can also be applied along arbitrary axes. Fast-switchable second-order shims would allow the quadratic phase to be applied along any axis—and indeed for any region in the body—and would remove the restriction of a nonselective excitation as the shim offsets need not be present during the RF excitation pulse. Our use of a nonselective excitation led us to choose the z-axis as the readout direction for the
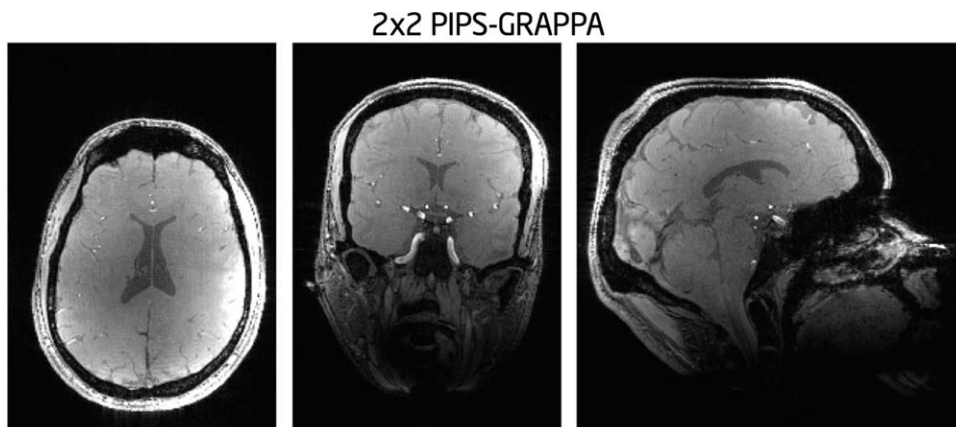
2x2 PIPS-GRAPPA

FIG. 8. Orthographic views of the PIPS-GRAPPA reconstruction of the 2 × 2 phase-scrambled undersampled data to demonstrate the effectiveness of the method throughout the brain.

3D-gradient encoding to avoid potential aliasing from signals below the head.

In this article, we found that PIPS-GRAPPA was able to out-perform PIPS-SENSE. This is likely due to the fact that we were able to make a simple iterative version of PIPS-GRAPPA, and therefore be more robust to the residual aliasing of high spatial frequencies which is present in the windowed convolution reconstruction. If a particular application required a SENSE-like approach, then with further investigation it may be possible to develop an iterative version of PIPS-SENSE. Extension of existing iterative SENSE-based methods [e.g., (9,22)] to PIPS may be possible, but is nontrivial as the coil sensitivities need to be approximated by a small number of coefficients—which in our experience is less robust for high channel-count RF receive arrays.

There have been several recent publications reporting methods that can also be considered "calibrationless" parallel imaging techniques (6–9) as they seek, directly or indirectly, to derive coil sensitivities from the undersampled data themselves. However, all these methods use k-space trajectories which sample at the Nyquist frequency close to the k-space center to ensure that the algorithm will converge to the desired solution. The method presented here, however, uses the spreading of the signals in k-space to provide the initial information necessary to guide the reconstruction toward the desired solution and it is, therefore, no longer required to critically sample the center of k-space.

There has also been recent work demonstrating that signals spread using quadratic phase can improve the results of a compressed sensing reconstruction (23). The current method, however, relies on the regular and predictable aliasing patterns associated with Cartesian undersampling. When applying the convolution with the windowed chirp function, it is necessary for the true signal location to fall within the locus of the window of its starting location, and all aliased locations to fall outside this locus. The method as described is, therefore, incompatible with the pseudorandom undersampling typically used for compressed sensing—which is deliberately applied to create incoherent aliasing. Similarly, common non-Cartesian trajectories such as radial or spiral sampling patterns are also incompatible with the convolution-based PIPS method described here—but it is clear that the spread k-space signals will still contain information about the coil

sensitivities. Further work is required to determine how this information can best be used for an optimal reconstruction.

Regions where flow crosses contours of the quadratic phase will potentially have encoding errors, the magnitude of which will depend on the flow velocity and the particular method used to impart the quadratic phase (i.e., how much time such errors have to evolve). However, in most MR imaging flow occurs over a small fraction of the FOV and would not be expected to perturb the ability to determine the initial GRAPPA weights (or low-resolution coil sensitivities for SENSE). In principle, we also expect PIPS to be applicable to phase-sensitive techniques, as provided the phase gradients of interest can be considered small compared to the spatial derivatives of the applied quadratic phase for PIPS then the PIPS convolution reconstruction should still be expected to have the desired result.

A valid concern when modifying the signals with such a strong phase function is that image quality will be compromised as a result of the phase scrambling. For the images we presented, the quadratic phase was chosen so as to impart a shift in k-space of approximately quarter of k-space at the edge of the FOV. In this case, the situation is similar to a three-fourth partial Fourier acquisition in the local k-space perspective for voxels at the edge of the FOV (but without a reduction in the total number of k-space samples). The exact degree of signal loss will depend on the local spatial frequency content of the object being described—but is expected to be mostly benign until the quadratic phase is so strong that it approaches the drastic signal loss as the principal echo moves outside the acquired range of k-space (19,24). These local k-space shifts will also have an effect on the local resolution of the reconstructed image. It may prove worthwhile to investigate the possibility of modifying existing algorithms for partial Fourier reconstruction, such as Projections Onto Convex Sets (POCS) (25), to properly deal with these data. For our present implementation with weak quadratic prephasing, we would only expect a small loss of resolution equivalent to the commonly used zero-filling for partial Fourier acquisitions.

In parallel imaging, the *g*-factor is often calculated as a measure of the loss of SNR associated with the use of the parallel imaging reconstruction beyond the inevitable SNR loss associated with using fewer samples (2). For
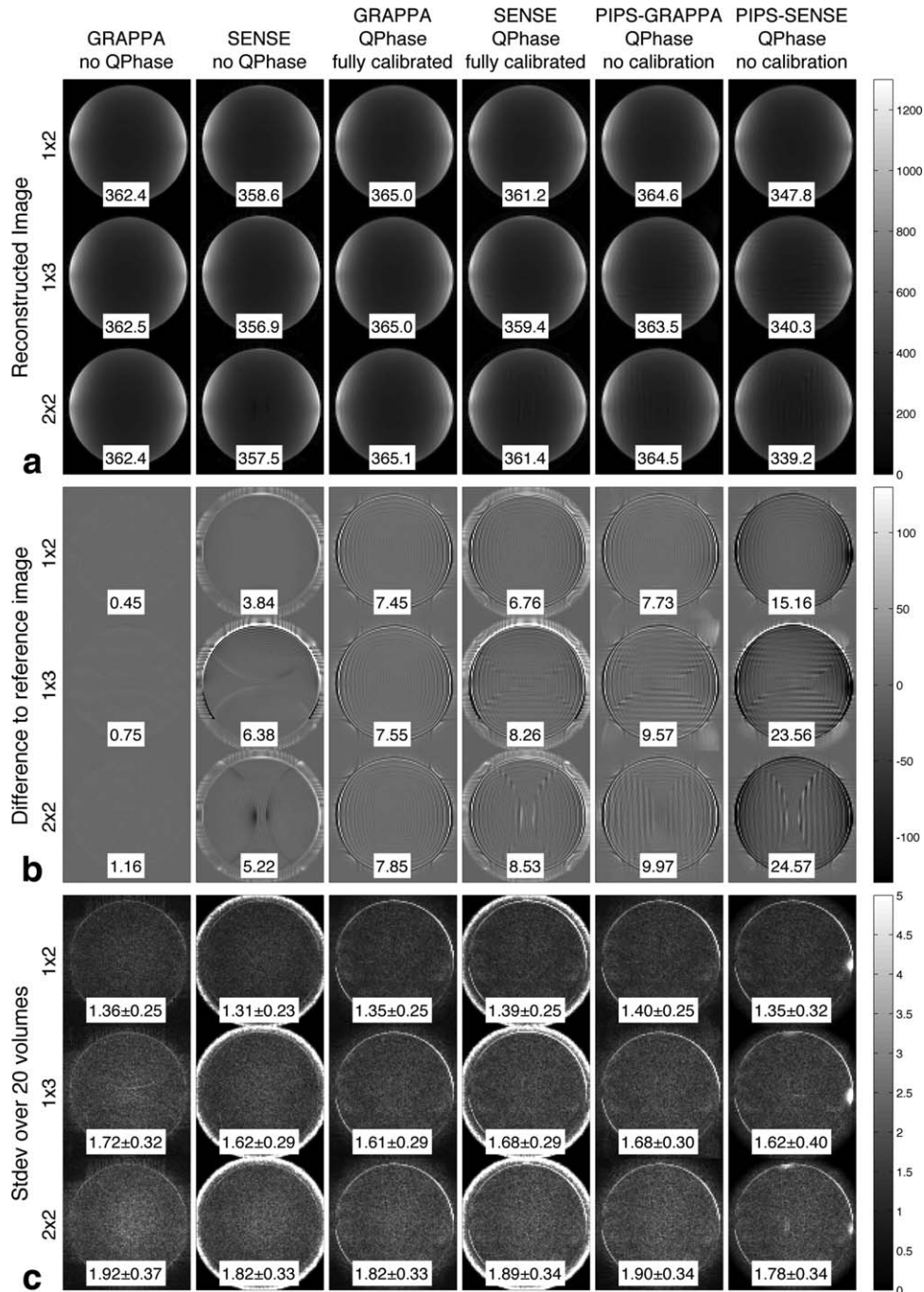
FIG. 9. Results from central slice of phantom SNR experiment. **a**: Mean reconstructed image at three acceleration factors (1×2, 1×3, and 2×2) using GRAPPA and SENSE with and without quadratic phase scrambling present, and PIPS-GRAPPA and PIPS-SENSE (which require phase scrambling). The mean signal (arbitrary units) within the phantom is also displayed. **b**: The difference between each reconstructed image and the sum-of-squares reconstruction of the fully sampled data without phase scrambling. The mean absolute difference within the phantom is also displayed. **c**: Standard deviation of the reconstruction across 20 acquired volumes. The mean and standard deviation of these values across the phantom are also displayed.

SENSE, the g-factor depends on the undersampling pattern, the coil sensitivity profiles and the noise correlation of the RF receive channels. We would, therefore, not expect the phase scrambling to have any influence on the g-factor as none of these will be affected. For GRAPPA, an equivalent definition has also been proposed, where the g-factor depends on the individual GRAPPA weights themselves (26). Further investigation would be required to determine whether the weights from phase-scrambled data should be expected to alter the GRAPPA g-factor in a predictable manner. Preliminary phantom measurements (Fig. 9) show no g-factor penalty associated with phase scrambling. We also observed that strong quadratic prephasing appears to make the images more sensitive to subject motion (e.g., the ringing toward the rear of the brain visible in Fig. 8).

This provides further motivation to reduce the required strength of the quadratic phase modulation.

CONCLUSIONS

In this work, we have presented a method for deriving coil sensitivity information to drive parallel imaging reconstructions directly from Cartesian undersampled data. In this proof-of-concept study based on a 3D acquisition, phase scrambling with a quadratic phase distribution was used to spread the signals in k-space, allowing a windowed convolution reconstruction to recover an image with aliasing suppressed, but reduced spatial resolution. Due to the smooth nature of coil sensitivities, however, this is sufficient to derive coil sensitivities for a PIPS-SENSE reconstruction, or the weights for a PIPS-GRAPPA kernel, which can then be applied to the undersampled data to reconstruct a full resolution alias-suppressed image.

ACKNOWLEDGMENT

REFERENCES

1. Sodickson DK, Manning WJ. Simultaneous acquisition of spatial harmonics (SMASH): fast imaging with radiofrequency coil arrays. Magn Reson Med 1997;38:591–603.

2. Pruessmann KP, Weiger M, Scheidegger MB, Boesiger P. SENSE: sensitivity encoding for fast MRI. Magn Reson Med 1999;42:952–962.

3. Griswold MA, Jakob PM, Heidemann RM, Nittka M, Jellus V, Wang J, Kiefer B, Haase A. Generalized autocalibrating partially parallel acquisitions (GRAPPA). Magn Reson Med 2002;47:1202–1210.

4. Jakob P, Griswold M, Edelman R, Sodickson DK. AUTO-SMASH: a self-calibrating technique for SMASH imaging. Magn Reson Mater Phys 1998;7:42–54.

5. Wang J, Kluge T, Nittka M, Jellus V, Kuehn B, Kiefer B. Parallel acquisition techniques with modified SENSE reconstruction (mSENSE). In 1st Workshop on Parallel MRI: Basics and Clinical Applications, Würzburg, Germany, 2001. p. 92.

6. Majumdar A, Ward RK. Calibration-less multi-coil MR image reconstruction. Magn Res Imaging 2012;30:1032–1045.

7. Lustig M. Post-Cartesian calibrationless parallel imaging reconstruction by structured low-rank matrix completion. In Proceedings of the 19th Annual Meeting of ISMRM. Montreal, Canada, 2011. p. 483.

8. Trzasko JD, Manduca A. Calibrationless parallel MRI using CLEAR. In Conference Record of the Forty Fifth Asilomar Conference on Signals, Systems and Computers (ASILOMAR), IEEE, Pacific Grove, California, USA, 2011. p. 75–79.

9. Uecker M, Hohage T, Block KT, Frahm J. Image reconstruction by regularized nonlinear inversion—joint estimation of coil sensitivities and image content. Magn Reson Med 2008;60:674–682.

10. Blaimer M, Breuer F, Heidemann RM, Müller M, Griswold MA, Jakob PM. Is parallel MRI without a priori information possible? In Proceedings of the 12th Meeting of ISMRM, Kyoto, Japan, 2004. p. 2417.

11. Wedeen VJ, Chao YS, Ackerman JL. Dynamic range compression in MRI by means of a nonlinear gradient pulse. Magn Reson Med 1988; 6:287–295.

12. Maudsley A. Dynamic range improvement in NMR imaging using phase scrambling. J Magn Reson 1988;76:287–305.

13. Pipe JG. Spatial encoding and reconstruction in MRI with quadratic phase profiles. Magn Reson Med 1995;33:24–33.

14. Ito S, Yamada Y. Alias-free image reconstruction using Fresnel transform in the phase-scrambling Fourier imaging technique. Magn Reson Med 2008;60:422–430.

15. De Graaf RA, Brown PB, McIntyre S, Rothman DL, Nixon TW. Dynamic shim updating (DSU) for multislice signal acquisition. Magn Reson Med 2003;49:409–416.

16. Schultz G, Ullmann P, Lehr H, Welz AM, Hennig J, Zaitsev M. Reconstruction of MRI data encoded with arbitrarily shaped, curvilinear, nonbijective magnetic fields. Magn Reson Med 2010;64:1390–1403.

17. Zaitsev M, Schultz G, Hennig J. Extended anti-aliasing reconstruction for phase-scrambled MRI with quadratic phase modulation. In Proceedings of the 17th Annual Meeting of ISMRM, Honolulu, Hawaii, USA, 2009. p. 2859.

18. Zaitsev M, Hennig J. Reference-free parallel imaging with phase scrambling (PIPS). In Proceedings of the 17th Annual Meeting of ISMRM, Honolulu, Hawaii, USA, 2009. p. 2676.

19. Witschey W, Cocosco CA, Gallichan D, Schultz G, Weber H, Welz AM, Hennig J, Zaitsev M. Localization by nonlinear phase preparation and k-space trajectory design. Magn Reson Med 2012;67:1620–1632.

20. Zhao T, Hu X. Iterative GRAPPA (iGRAPPA) for improved parallel imaging reconstruction. Magn Reson Med 2008;59:903–907.

21. Koch KM, McIntyre S, Nixon TW, Rothman DL, de Graaf RA. Dynamic shim updating on the human brain. J Magn Reson 2006;180:286–296.

22. Ying L, Sheng J. Joint image reconstruction and sensitivity estimation in SENSE (JSENSE). Magn Reson Med 2007;57:1196–1202.

23. Puy G, Marques JP, Gruetter R, Thiran J-P, Van De Ville D, Vandergheynst P, Wiaux Y. Spread spectrum magnetic resonance imaging. IEEE Trans Med Imaging 2012;31:586–598.

24. Wedeen VJ, Weisskoff RM, Poncelet BP. MRI signal void due to in-plane motion is all-or-none. Magn Reson Med 1994;32:116–120.

25. Haacke EM, Liang Z-P, Boada F. Image reconstruction using projection onto convex sets, model constraints, and linear prediction theory for the removal of phase, motion, and Gibbs artifacts in magnetic resonance and ultrasound imaging. Opt Eng 1990;29:555–566.

26. Breuer FA, Kannengiesser SAR, Blaimer M, Seiberlich N, Jakob PM, Griswold MA. General formulation for quantitative G-factor calculation in GRAPPA reconstructions. Magn Reson Med 2009;62:739–746.